MAX-PLANCK-GESELLSCHAFT

Handbook of Heterogeneous Catalysis, Vol.3, (2008) 1462-1479

5.2.2. Dynamics of surface reactions

G. Ertl

5.2.2.1 Introduction

Catalysis concerns the rate of a chemical reaction which is usually expressed as a function of the concentrations of the species involved in the reaction and a set of rate constants k_i which depend on temperature T. Within the framework of transition state theory (TST) [1], which forms the basis of chemical kinetics, the latter are given by

$$k_i = \frac{k_B T}{h} \cdot e^{\Delta S^* / R} \cdot e^{-E^*/RT} \qquad (1)$$

whereby E* is the activation energy (= the height of the energy barrier along the 'reaction coordinate', i.e. the path with minimum energy with respect to all other degrees of freedom for nuclear motion). The term $\frac{k_B T}{h} \cdot e^{\Delta S^*/R}$ (with k_B = Boltzmann's constant and h = Planck's constant) denotes the 'preexponential' factor and is determined by the entropy difference ΔS^* between the transition state and the initial state.

The basic idea of TST consists in the assumption that at all stages along the reaction coordinate thermal equilibrium is established, so that the temperature (T) is the only essential (macroscopic) parameter. This requires that energy exchange between the various degrees of freedom of the particle interacting with the surface and the heat bath of the solid occur much faster than the process of chemical transformation. This chapter will discuss effects, for which this condition is not fulfilled and hence the observed phenomena are governed by dynamics rather than by kinetics.

5.2.2.2 Energy exchange between adsorbate and solid

An estimate of the typical energy relaxation time of a chemisorbed particle, t_{relax}, can be obtained from observations with scanning tunneling microscopy (STM) [2,3]. Thermally activated dissociation of O_2 molecules chemisorbed as peroxo-like species on a Pt(111) surface leads to the formation of pairs of chemisorbed O atoms. If the temperature is low enough (≤ 180 K), these atoms are not mobile once they are at thermal equilibrium with the solid and hence they do not change their positions over longer periods of time. Interestingly, it is found that the adatoms resulting from dissociation of an individual O_2 molecule are not located on adjacent sites, but are rather separated by 5 – 8 Å from each other. This effect is a consequence of the finite time needed for damping the adsorption energy into the heat bath of the solid. As illustrated by the schematic potential diagram of Fig. 1, dissociative chemisorption

along the reaction coordinate comprises mutual separation of the two atoms parallel to the surface plane. Obviously this does not occur along the solid line representing the ground state, but along the dotted line involving 'hot' adatoms. From the distance <l> traversed until thermal equilibrium is reached and from the mean velocity (derived from the chemisorption energy released), an average relaxation time on the order $t_{relax} \approx 3x10^{-13}$ s is estimated. It can thus be concluded that for surface processes occurring on a time scale $<10^{-12}$ s the concept of TST will not longer be valid. This will be the case for processes in which coupling of the particle to the heat bath of the solid is shorter ,i.e. in cases of collision induced adsorption or reaction as well when product molecules are directly released into the gas phase. On the other hand, the formation of 'hot' adparticles in the course of dissociative chemisorption as just discussed is expected to be of quite general nature and will be further alluded below. A quite dramatic effect of this kind (which is still not fully explained theoretically) has been observed with the dissociative adsorption of oxygen on Al(111) where the 'hot' adatoms travel by quite long distances across the surface before they come to rest [4]. The role of such elementary processes in catalytic reactions has still to be explored and some further aspects will be discussed below.

The full line in Fig. 1b describes the evolution of the reactant (free O_2 molecule) to the product (chemisorbed O atoms) along the electronic ground state as determined by the Born-Oppenheimer potential energy surface which is obviously not perfectly fulfilled. We may therefore ask for typical time constants for the exchange of energy between the degrees of freedom of the adsorbate and the solid substrate. Within the latter these are the lattice

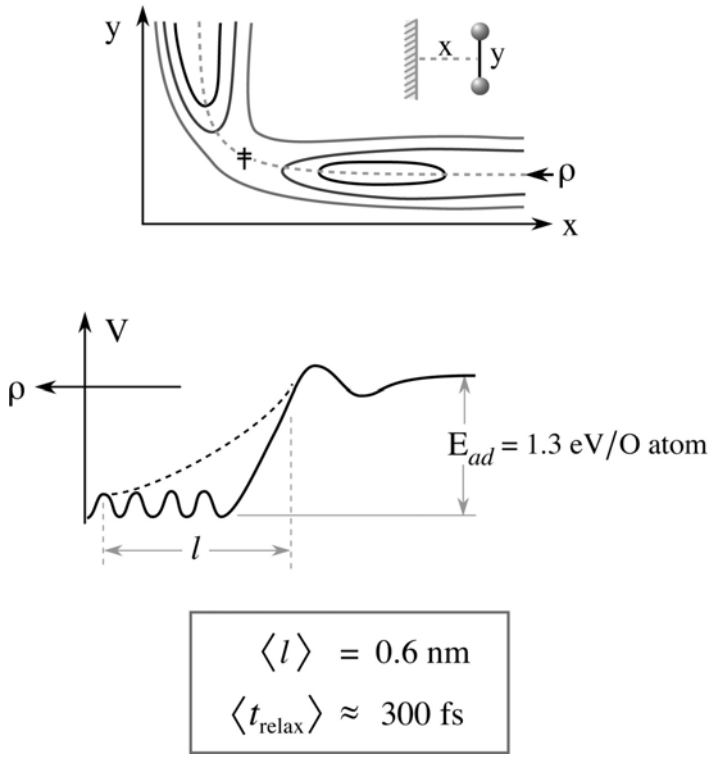

Fig.1: Schematic potential diagram (a: two-dimensional, b: one-dimensional) for dissociative adsorption of a diatomic molecule such as O^2 on Pt(111).

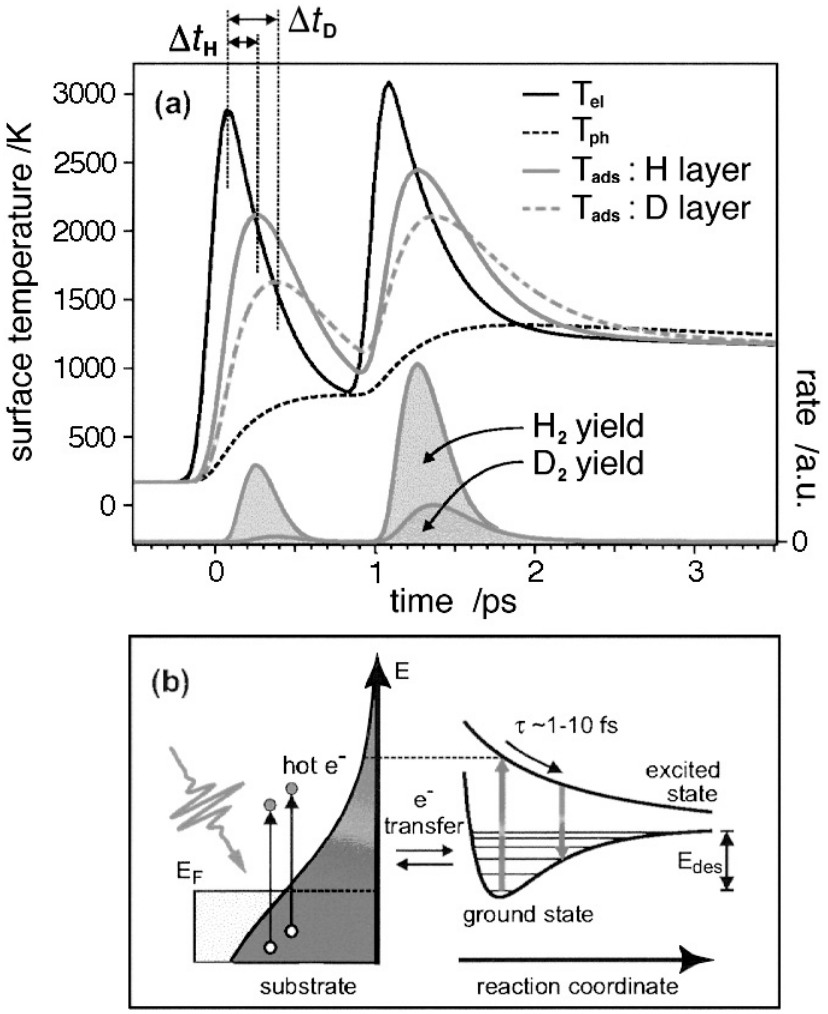

Fig. 2: fs-laser induced associative desorption of hydrogen from Ru(0001) [5].
a: Variation of the electronic, phonon and adsorbate temperatures with time after absorption of two pulses separated by 1 ps
b: Illustration of the electronic processes following light absorption

vibrations (phonons) and the conduction electrons. Experimental access to this question could be obtained by rapid absorption of an infrared pulse by the conduction electrons of a metal surface [5]. A Ru(0001) surface was covered by dissociatively adsorbed H (D) atoms which could in turn be associatively desorbed by thermal desorption spectroscopy (TDS) with a mean kinetic (thermal) energy of around 350 K. If instead the surface was irradiated with 130 fs long IR pulses at 800 nm the desorbing molecules exhibit much higher kinetic energies around 2000 K, and the yield of H_2 with a single shot is about 10 times that for D_2. Further detailed experiments [6] and their analysis revealed the following picture as illustrated by Fig. 2: Absorption of the photons by the conduction electrons creates hot electrons above the Fermi level E_F which rapidly ($\leq$ 100 fs) equilibrate internally to an electron temperature T_{el} and subsequently couple to the lattice characterized by its phonon temperature T_{ph}. The occupation of electronic states above E_F is governed by Fermi-Dirac statistics (Fig. 2b). As a consequence, an adsorbate derived affinity level above E_F may become transiently populated, whereby the system is transferred to an electronically excited state. The gradient on this potential causes nuclear motion, eventually leading (by multiple excitation – relaxation steps between ground and excited state) to desorption via a nonadiabatic mechanism based on coupling between electronic and nuclear degrees of freedom. Because of the mass difference between H and D the motion of the latter species on the excited potential is slower and hence its desorption yield smaller. Fig. 2a depicts the variation of the different

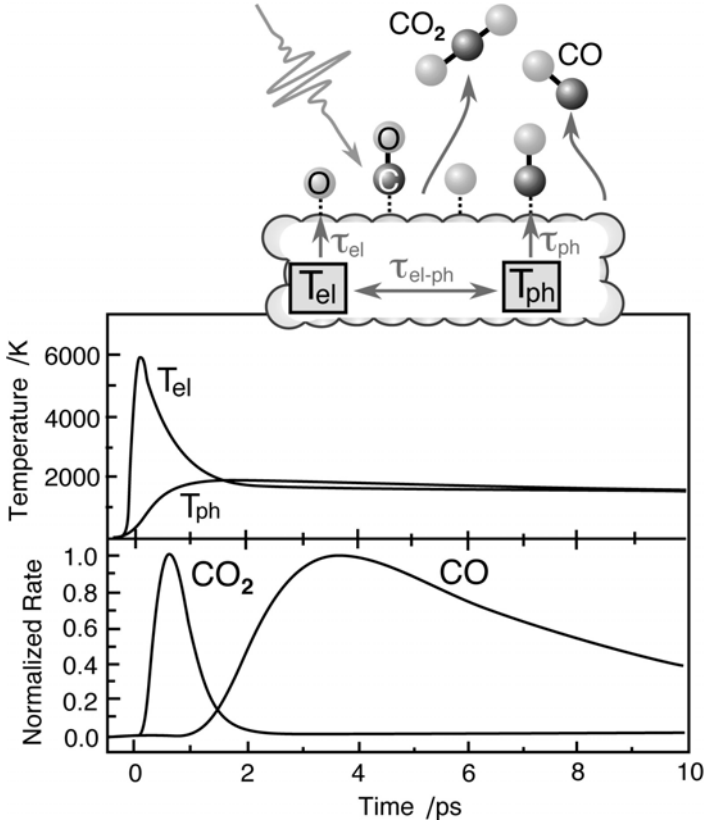

Fig 3: Time evolution of a Ru(0001) surface covered by coadsorbed O+CO after irradiation with an intense infrared laser pulse of 130 fs duration. Variation of the electron and phonon temperatures, T_{el} and T_{ph}, respectively with time, leading to CO desorption and CO^2 evolution [7].

temperatures (T_{el}, T_{ph}, T_{ad} (H) and T_{ad} (D)) with time for two subsequent pulses. It can be seen that these equilibrate within about 1 ps to the common lattice temperature T_{ph} so that thermal equilibrium is reached. It can thus be concluded that *processes on a timescale ≥1 ps during which the adsorbate is closely coupled to the solid proceed on the electronic ground state and can be safely described by TST*. Manifestations of the breakdown of this concept to be discussed below are usually characterized by shorter coupling times.

An example for which separation of the time scales for electron and phonon excitation had direct consequences on the catalytic yield was found with CO-oxidation on a Ru(0001) surface onto which O+CO were coadsorbed [7]. When the temperature of the sample was continuously increased by heating, only desorption of CO, but no formation of CO_2 was observed. This situation changed if the just mentioned fs light pulses (800 nm, 130 fs) were applied: now both CO and CO_2 came off the surface. Two-pulse correlation experiments with varying delay times between subsequent pulses (such as with Fig. 2a) revealed that the relaxation time for the decay of the excitation responsible for CO desorption was on the order of 20 ps, but was much shorter (~1 ps) for CO_2 formation. As shown in Fig. 3, CO_2 formation takes primarily place during the first picosecond after absorption of the IR pulse by the valence electrons when T_{el} reaches values up to 6000 K, whereas desorption starts only later with the increase of T_{ph}. The latter process is associated with a (thermal) activation energy of 0.8 eV, while that for CO_2 formation is 1.8 eV. This explains why with normal heating CO desorption takes place before recombination O+CO occurs. The formation of hot electrons about E_F during the laser shot, however, causes substantial population of an O 2p-derived level which is antibonding with respect to the adsorbate-substrate bond. Coupling to the nuclear motion then in-

itiates CO_2 formation. For adsorbed CO, on the other hand, the lowest lying empty level (derived from the CO 2π*-orbital) is located about 5 eV above E_F and is thus much too high in energy to become substantially populated by electronic heating, and hence CO desorption takes place from the electronic ground state through coupling to phonon excitations.

The variation of the C-O stretching frequency of CO adsorbed on Ru(0001) with surface temperature during fs-laser heating could in fact be directly followed by time-resolved sum-frequency spectroscopy [8]. Parallel to heating up the surface by a fs-IR pulse as before, part of this radiation was mixed with a visible up-conversion pulse. A set of resulting time-resolved spectra with varying pump-probe delays is reproduced in Fig. 4. The continuous broadening and frequency shift can be attributed to the temperature dependence of the C-O stretch band, caused by anharmonic coupling to a frustrated translational mode and other low lying modes of the adsorbate. Thermally induced increase of the amplitude of this motion displaces the CO molecules from its on-top position towards a bridge position, where it has a lower C-O stretch frequency. After longer (>100 ps) times the sample has cooled down and the band is centered at its original position, however with lower intensity which reflects partial desorption. In this way it is demonstrated how the internal degrees of freedom of an adsorbate are in thermal equilibrium with the phonon heat bath even during reaction (desorption). Quite analogous conclusions were reached in a similar, more recent study with the system $CO/Ru(10\bar{1}0)$ [9].

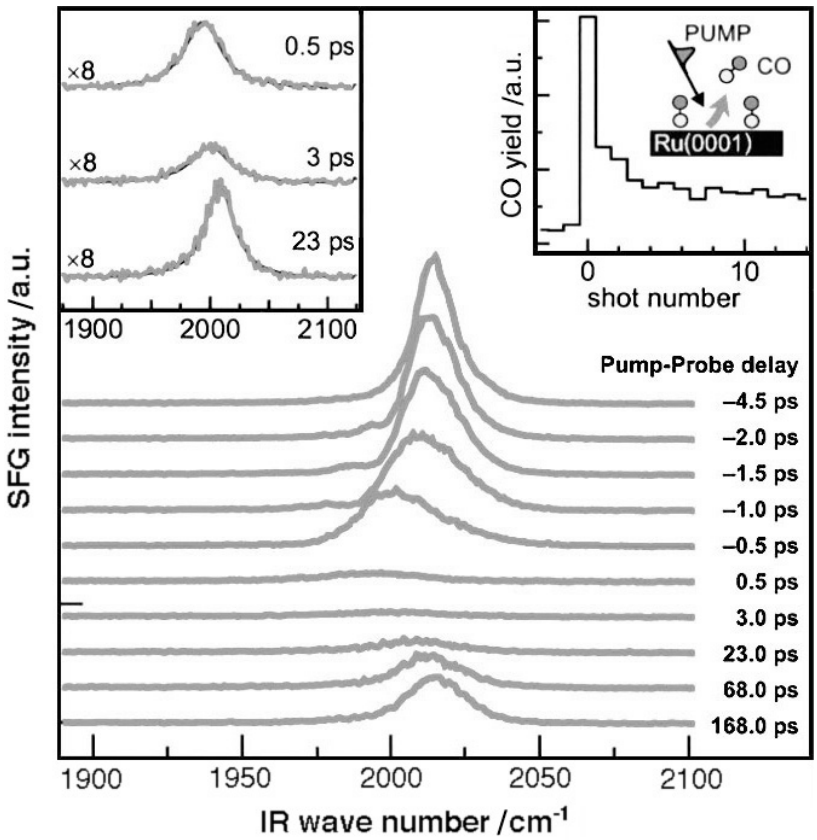

Fig. 4: Transient SFG spectra from the C-O stretch vibration of CO adsorbed on Ru(0001) after rapidly heating the surface from 300 to 800 K by an intense fs laser pulse and subsequent cooling [8].

5.2.2.3 Limitations of transition state theory

The conclusion that chemisorbed particles are in thermal equilibrium with the solid even on a ps time scale while strongly coupled to the surface may, however, break down if the molecules are released into the gas phase and we consider the energy contents of the various degrees of freedom after desorption. This was verified for the CO/Ru(0001) system when the translational energy of the (thermally) desorbing molecules was evaluated from time-of-flight (TOF) spectra [10]. The measured TOF data were converted into the mean translational energy $<E_{trans}>$ and translational temperature $<E_{trans}>/2k_B$ (k_B = Boltzmann's constant) of the desorbing molecules. As shown in Fig. 5a, $<E_{trans}>/2k_B$ as a function of the laser fluence F is always considerably smaller than the actual temperature in the adsorbed state $<T_{ads}>$. The variation of T_{ads} together with the electron and phonon temperatures, T_{el} and T_{ph}, and the desorption rate R as a function of time during such a fs-laser pulse desorption experiment is shown in fig. 5b.

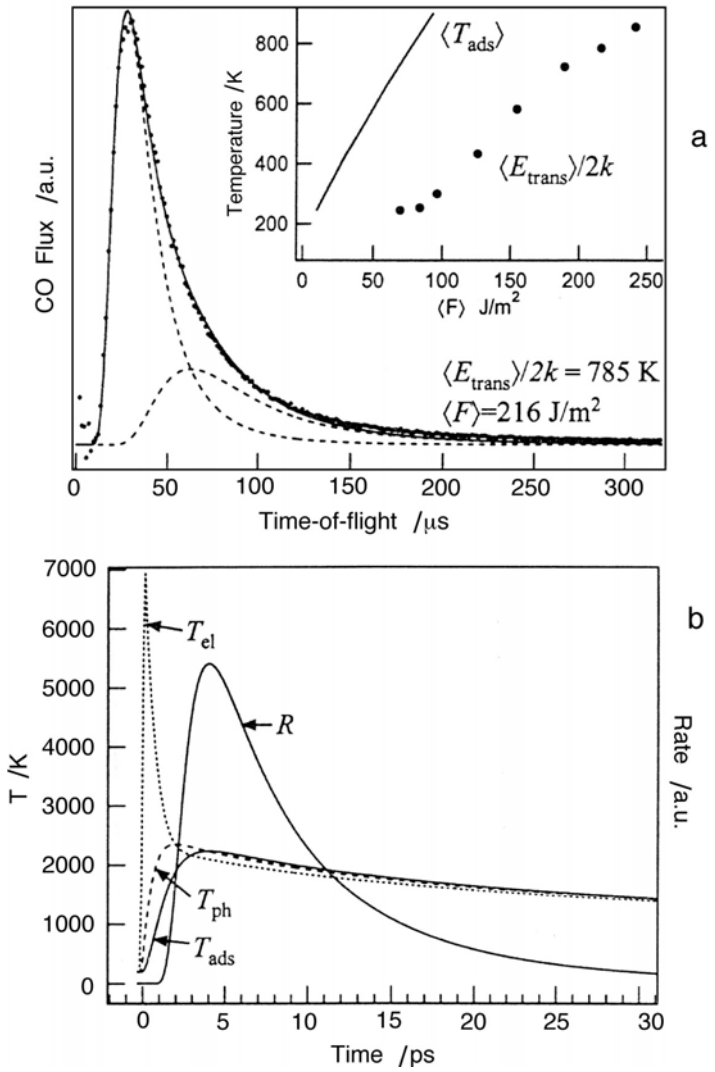

Fig. 5: Desorption of CO from Ru(0001) after irradiation with an intense fs laser pulse [10].
a: Time-of-flight (TOF) data for a typical laser fluence <F>. The inset shows the variation of the mean translational energy $<E_{trans}>/2k$ and of the adsorbate temperature Tads with laser fluence <F>
b: Typical transients for the temperatures of the electrons T_{el}, phonons T_{ph}, and adsorbate T_{ad}, respectively, together with the resulting desorption rate R as a function of time.

This effect of "cooling in desorption" is quite common [11] and extents also to other degrees of freedom. For example, Fig. 6 demonstrates that the mean rotational temperature of NO molecules desorbing form a Pt(111) surface is equal to the surface temperature only up to about 400 K and then levels off because of incomplete excitation of the rotational motion during the desorption event [12].

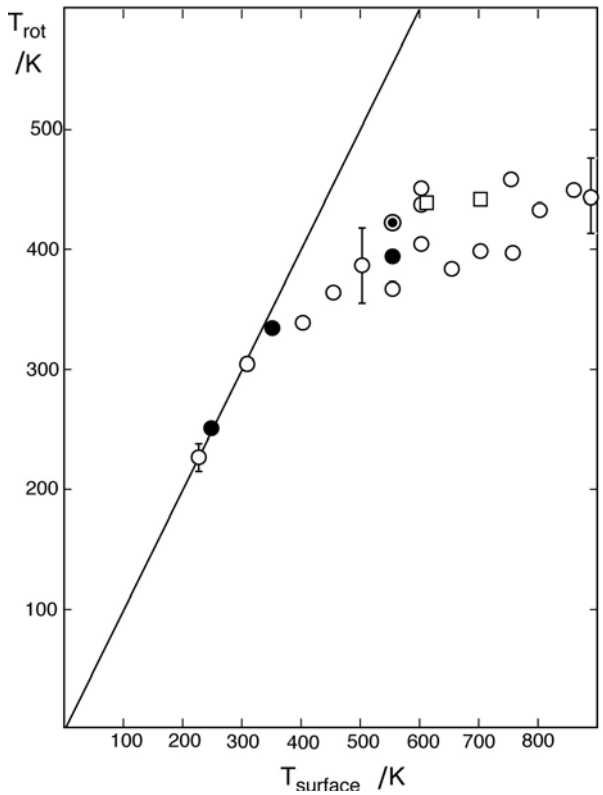

Fig. 6: Variation of the rotational temperature T_{rot} of NO molecules desorbing from a Pt(111) surface as a function of surface temperature $T_{surface}$. The straight line represents $T_{rot} = T_{surface}$ [12]

5.2.2.4 Sticking

Modeling of the kinetics of a catalytic reaction is frequently based on a 'hit and stick' model for adsorption derived from the Langmuir adsorption isotherm. If a particle impinging from the gas phase hits an unoccupied adsorption site, it sticks (= becomes adsorbed). The situation for dissociative adsorption of H_2 on Ni(110) and Ni(111) at zero coverage (s_o) is illustrated by Fig. 7 [13]. Fig. 7a shows that s_o for H_2 molecules with constant kinetic energy (64 meV) on Ni(111) is independent of surface temperature and rather small, but increases continuously with the normal component of the translational energy (Fig. 7b). In view of the potential diagram of Fig. 1 these data suggest that there exists an activation barrier of about 0.1 eV for dissociation that, however, cannot be overcome by coupling to the heat bath of the solid since the interaction time during direct collision is too short, but instead requires high enough translational energy of the impinging molecules. With Ni(110), obviously such a barrier is negligible, since s_o is close to unity, independent of kinetic energy and surface temperature. For this process TST obviously fails because the time of interaction and energy exchange between the impinging molecule and the solid surface is not long enough.

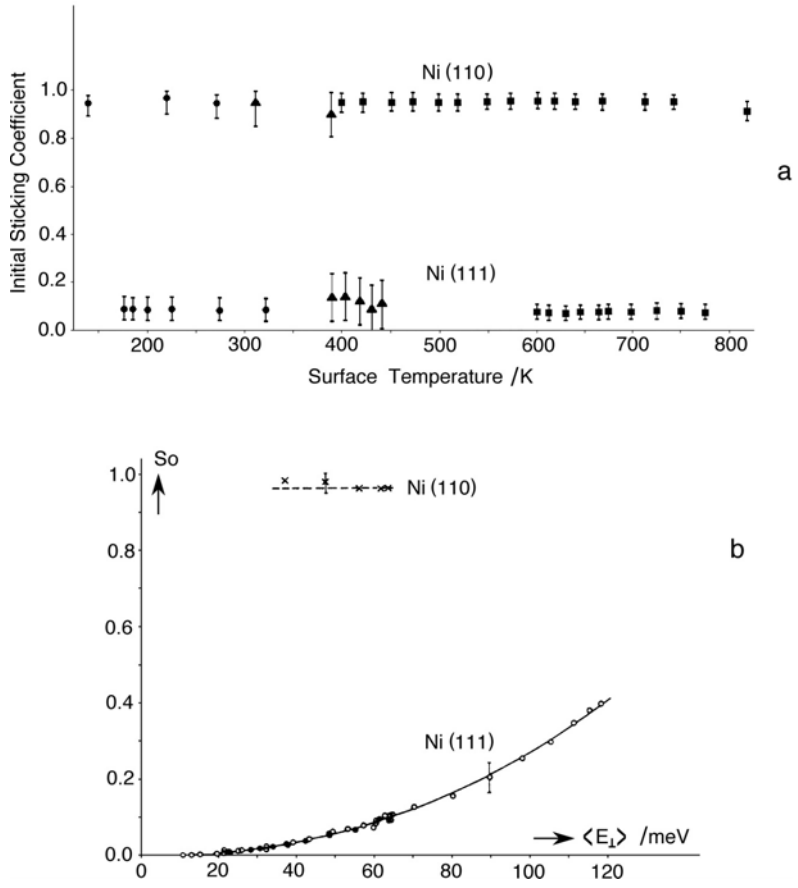

Fig. 7: The initial sticking coefficient s_O for dissociative adsorption of H_2 on Ni(110) and Ni(111) surfaces [13].
a: as a function of surface temperature
b: as a function of the incident kinetic energy

Dissociative adsorption of hydrogen molecules on copper surfaces served as benchmark systems for these types of effects. Molecular beam experiments were performed with systematic variation of the translational energy and combined with probing the populations of vibrational and rotational levels, the latter even with selection of the polarization ('cartwheel' vs 'helicopter') [14-16]. The detailed experimental findings prompted the evaluation of sophisticated potential energy surfaces and theoretical modeling of the dynamics of this prototype reaction [17]. Further details will be presented below in connection with effects associated with the reverse process, namely associative desorption.

Dissociative adsorption of methane is another interesting example in which bond breaking occurs by collision of the impinging molecule with the surface [18]. Again, the dissociation probability increases with the translational energy normal to the surface, while the surface temperature is without noticeable effect. Additional experiments demonstrated that excitation of the bending and umbrella vibrational modes had a similar effect as an increase of the translational energy. This suggests that in fact deformation of the methane molecule during collision is decisive for dissociation, and also explains why attempts to promote this process by preceding optical excitation had little effect [19]. On the other hand, experiments with NO excited to higher vibrational states revealed a much higher probability for dissociative adsorption on Cu(111) than in the vibrational ground state [20].

Another example relevant to an important technological process demonstrates the actual complexity: For catalytic ammonia synthesis, dissociative nitrogen adsorption is the rate limiting step whereby the Fe(111) surface exhibits the highest activity [21]. The sticking coefficient for this step is very low and increases with surface temperature, from which a sequential mechanism through molecular precursor states was concluded [22]. Molecular beam experiments, on the other hand, revealed a pronounced increase of the sticking coefficient with kinetic energy of the incident N_2 molecules, suggesting the operation of a 'direct' collision-induced mechanism [23]. A detailed theoretical analysis resolved this apparent contradiction [24]. There exist in fact two dissociation channels, one precursor-mediated with low energy barrier, but high entropy barrier (thus explaining the overall low sticking coefficient) which dominates under usual synthesis conditions so that also TST is applicable, and another, direct one with high activation barrier which is favoured in the molecular beam experiments with high kinetic energies of the impinging molecules.

Even non-dissociative (molecular) adsorption may be associated with an activation barrier, if e.g. the process proceeds via a physisorbed into a chemisorbed state (trapping-mediated adsorption). In the system O_2/Pt(111), for example, the molecule may be either chemisorbed in a superoxo-like or peroxo-like state [25]. In molecular beam experiments it was then found that at low kinetic energies both types of surface species are formed, while at higher kinetic energies the more strongly held peroxo-like species is favoured, thus reflecting correlations between incident translational energy and preferred trajectories for adsorption [26].

In general, even for nondissociative adsorption without an activation barrier in the entrance channel the (initial) sticking coefficient will deviate (perhaps only very slightly) from unity and decreases both with increasing kinetic energy and increasing surface temperature because of incomplete energy exchange, as was explored in more detail in state-resolved experiments and classical trajectory calculations [27].

Under the high-pressure conditions of 'real' catalysis, both the catalyst and the gas phase will be at the same temperature so that effects arising from restricted energy exchange will be masked. Nevertheless, these phenomena enter the evaluation of the kinetic parameters so that their analysis is of relevance for better understanding of catalytic activity.

5.2.2.5 Collisions-induced surface reactions

Apart from sticking also other surface reactions may be affected by direct impact of particles from the gas phase. For example, dissociative adsorption of CH_4 may not only be promoted by high enough kinetic energy of the impinging methane molecules, but an already adsorbed adlayer may also be brought to dissociation by impact of Ar atoms ("chemistry with a hammer") [36,37]. In contrast to dissociation by direct impact, in this case the reaction probability does not simply scale with the normal component of the kinetic energy of the Ar atoms. Instead it was concluded that first the collision energy is transferred to the adsorbed CH_4 molecule where it is redistributed and causes dissociation or desorption with even higher probability. Similar effects were also found in a careful study on hydrocarbons adsorbed on Au(111) and subject to beams of Xe atoms with varying kinetic energies [88]. Collision-induced reactions were also observed with chemisorbed systems [39-41]. For O_2 chemisorbed on Ag(110) or Pt(111) impact of Xe atoms causes desorption and dissociation with a common threshold energy of 0.9 and 1.2 eV, respec-

tively. These values are considerably higher than the respective thermal activation energies. Equal thresholds for both desorption and dissociation are presumably the consequence of rapid energy exchange between the different modes of nuclear motion (viz., the O-O vibration leading to dissociation and the M-O_2 vibration causing desorption).

If a layer of coadsorbed CO+O_2 is bombarded by Xe atoms also the release of CO_2 is observed [40]. It is likely that this is a secondary effect: Dissociation of adsorbed O_2 causes the transient formation of 'hot' O adatoms exhibiting a high reaction probability with neighboring CO as will be discussed further in the next section.

5.2.2.6 Langmuir-Hinshelwood vs. Eley-Rideal mechanisms

The preceding two sections lead directly to a classical problem in heterogeneous catalysis for a reaction A+B: In the Langmuir-Hinshelwood (LH) mechanism both species are in the adsorbed state and fully equilibrated with the surface, while with the Eley-Rideal (ER) mechanism an adsorbed species A reacts with particles B directly impinging from the gas phase.

Generally, most surface catalytic reactions are considered to proceed via the LH mechanism. Experimental verification is obtained in experiments in which, after adsorption of the reactants A+B, the gas phase is removed and the sample temperature continuously increased until the product molecules AB come off (temperature programmed reaction spectroscopy = TPRS). Specifically, the LH mechanism is operating if the time delay for product formation is long enough (≥10 ps) for reaching thermal equilibrium at the surface. For the CO+O reaction on Pd(111) this delay time was determined in molecular beam experiments down to about 10^{-4} s, and from these data the activation energy for the LH reaction was derived [42].

Reactions involving hot adatoms as discussed before represent obviously an intermediate situation between the two limiting cases LH and ER in so far, as the reactants are not in complete thermal equilibrium with the surface (LH), but the reaction, on the other hand, does not take place by direct collision without (at least partial) previous accommodation (ER).

Clear cases for the operation of the (pure) ER mechanism are still rather scarce and so far restricted to reactions involving the impact of *atoms* (i.e. energetic species) onto the surface.

With CO oxidation on Pt(111), the first evidence for non-LH behavior was found for beams of O *atoms* (impinging together with CO molecules) onto the surface [43]. (The reaction with O_2 molecules, on the other hand, proceeds clearly via the LH mechanism). If the energy content of the product molecules was probed by infrared chemiluminescence, CO_2 molecules formed by impact of O atoms exhibited a higher degree of internal excitation than when O_2 molecules were used, suggesting some kind of "memory" of the initial state of the reactants [44]. The suggested operation of an ER mechanism in this case [45] was supported by classical trajectory calculations [46]. There it was found that most reactive events occurred within the first few ps after impact. However, a substantial fraction of product molecules is also formed after somewhat longer times and are hence better classified as hot adatoms events.

The most detailed investigations on the operation of an ER mechanism were performed with reactions involving the collision of an incident hydrogen atom onto an adsorbed species, such as $H + D_{ad} \rightarrow HD$. The energy balance for this process reads $E_{HD} = E_{diss}(HD) + E_{kin}(H) - E_{ad}(D)$ which amounts to about 2.3 eV for Cu(111). State-resolved experiments revealed in this case such an amount of energy carried away by the HD molecules in their translational, vibrational, and rotational degrees of freedom [47,48]. Similarly, the reaction $D + D_{ad} \rightarrow D_2$ on Ni(110) was reported to produce rotationally and vibrationally excited molecules [49], and the conclusion of an ER mechanism was supported by theoretical results [50,51].

However, experiments with the H+D_{ad} reaction on Ni(110) revealed not only HD as product molecules but also D_2 [52]. In addition, it was found that the rate of HD formation was not simply proportional to the surface coverage with D as expected for a pure ER mechanism [53,54]. Therefore a more complex sequence of elementary steps was proposed as sketched in Fig. 8 [53]: In addition to a pure ER mechanism (a), a fraction of the incident H atoms may become adsorbed causing a modified ER mechanism (b). In addition, some of the impinging H atoms may become trapped (but not completely accommodated) as hot adatoms and then either react with D_{ad} (c) or transfer their energy to adsorbed D atoms which become thus excited and may even react further to D_2 (d). Computer simulations revealed that all experimental observations may be (qualitatively) rationalized by this concept [55] which later was developed further [56]. The same group investigated in great detail also a series of other reactions of this type, including the abstraction by H atoms of chemisorbed D atoms from graphite [57], Si(111) [58], Ag(100) and (111) [59], but also of chemisorbed O from Cu [60-62] or Pt(111) [63]. The general conclusion is that the original ER mechanism as proposed long ago [64] only hardly operates in its pure form, even not in reactions involving atomic (i.e. energetic) reactants, but that the actual situation is usually more complex.

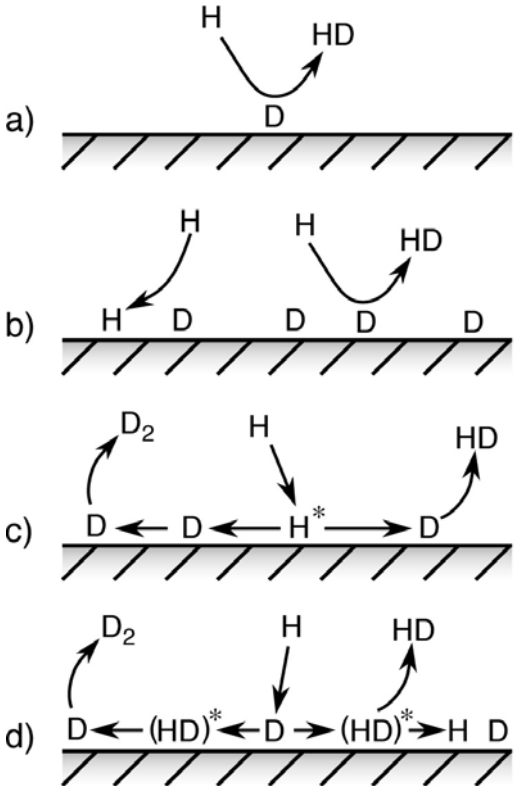

Fig. 8: Proposed reaction steps involved in the interaction of H atoms iminging onto a D covered surface [53].

5.2.2.7 'Hot' adparticles

Already Langmuir [28] had observed that the sticking coefficient in non-dissociative adsorption does not necessarily decrease linearly with coverage as expected from the "hit and stick" model, and he attributed this effect to the intermediate formation of mobile surface species. The 'precursor' model [29,30] assumes that an incident particle can also be weakly trapped on an already occupied site. There, it is thermally accommodated and exhibits high mobility during a limited surface residence time during which it can reach a free chemisorption site with finite probability. This 'precursor' particle is considered to be in thermal equilibrium with the surface. There exist, however, a number of observations where this is no longer the case: These 'hot' adparticles are trapped on the surface for a short time before they reach thermal equilibrium, during which period they may give rise to novel dynamic effects.

Tully [11] had realized in trajectory calculations for the interaction of noble gas atoms with a Pt surface that long after thermal equilibration of their normal component of kinetic energy, trapped molecules may slide across the surface over rather long distances before also the tangential component is equilibrated, thus confirming previous suggestions along the same line [31,32]. Qualitative rationalization is sketched in Fig. 9. An incident particle will first hit the repulsive part of the interaction potential and exchanges its adsorption energy only stepwise (Fig. 9a). Since the variation of the potential parallel to the surface is generally weaker than perpendicular to it the particle will travel some distance across the surface before it comes to rest (Fig. 9b). If along this path, however, it hits an already accommodated other particle with the same mass (Fig. 9c), energy transfer will be very efficient and the two particles will remain preferably attached to each other, provided that the surface temperature is low enough to prevent regular (i.e. thermally activated) diffusion.

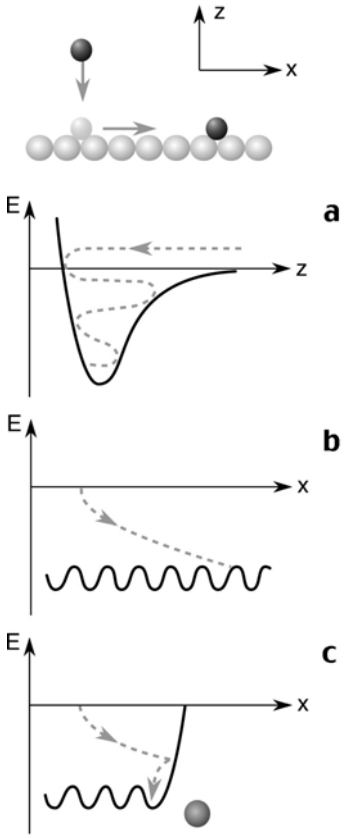

Fig. 9: Mechanism of the hot precursor model for adsorption.

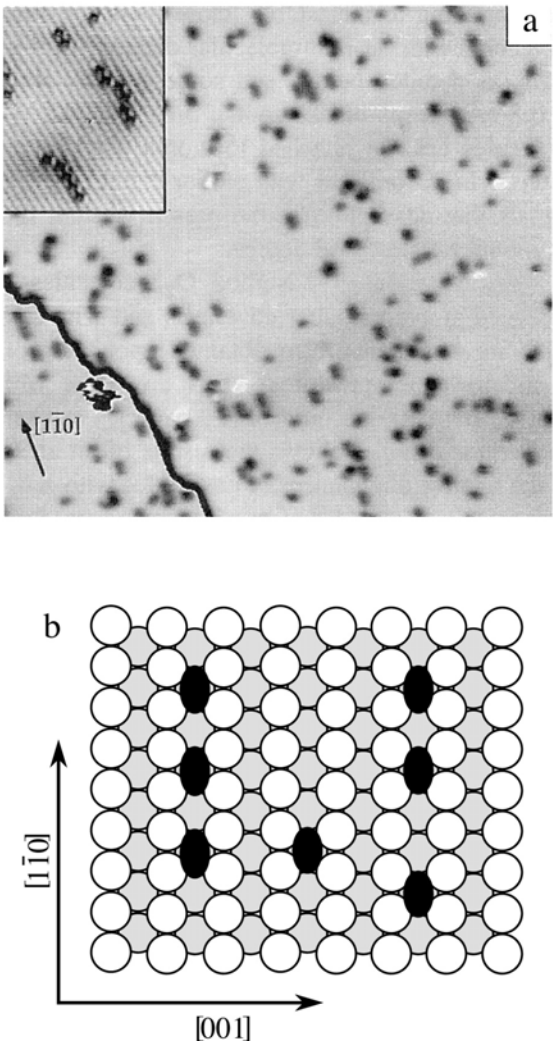

Fig. 10: STM data from (non-dissociative) adsorption of O_2 molecules on an Ag(110) surface at 65 K, demonstrating the operation of the hot precursor model [33].
a: STM image 30x23 nm^2 after adsorption of 2% of a monolayer
b: Model with adsorbed O_2 molecules (black) and Ag atoms from the first (white) and second (grey) layer.

Experimental verification of this effect is demonstrated by the STM image of Fig. 10a [33]: About 2% of a monolayer (ML) O_2 molecules had been adsorbed on an Ag(110) surface at 65 K. At this low temperature no dissociation takes place and the thermal mobility is negligible. If the randomly impinging molecules would come to rest at their respective point of impact, the vast majority of them would be discernible as isolated adparticles which is however not the case. The inset of Fig. 10a shows a section with atomic resolution in which both the rows of Ag atoms along the $[1\bar{1}0]$-orientation and the adparticles (black dots) are resolved. Almost no isolated single adparticles are discernible, but rather agglomerates with typically 2 to 4 O_2 molecules with mutual separation of 2a along the $[1\bar{1}0]$-direction which is the energetically favourable configuration as sketched in Fig. 10b. This observation demonstrates directly the operation of the discussed 'hot' adparticle effect.

Such effects may not only result from transient incomplete accommodation of a particle trapped on the surface from the gas phase, but may also result from a reaction occurring on the surface. The dissociative adsorption of O_2 on Pt(111) [2,3] or Al(111) [4] as already discussed in sect. 5.2.2.2 belong into this category.

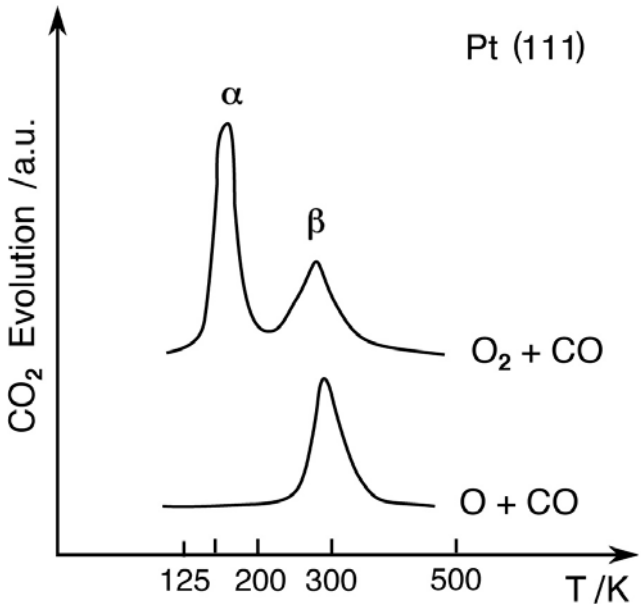

Fig. 11: Temperature-programmed reaction spectroscopy (TPRS) from a Pt(111) surface covered by CO and O (lower trace) and O_2 (upper trace), respectively [66].

These 'hot' adatoms are more energetic than they would be if accommodated with the surface and are hence also expected to be more reactive. Experimental evidence for such effects involving adsorbed oxygen was presented by Roberts et al. [34-36], and becomes even more pronounced in several studies on the oxidation of CO on platinum [65-67]. If O atoms and CO are coadsorbed on a Pt(111) surface, temperature-programmed reaction spectroscopy (TPRS) exhibits a peak of CO_2 formation (β) centered around 300 K as reproduced in Fig. 11 [66], arising from the regular Langmuir-Hinshelwood reaction $O_{ad} + CO_{ad} \rightarrow CO_2$ When, however, instead O_2 molecules were coadsorbed with CO at low temperatures, subsequent heating caused the appearance of an additional CO_2 peak at 150 K, just the temperature at which $O_{2,ad}$ dissociates and forms transient 'hot' adatoms with a lifetime of about 300 fs as discussed in sect. 5.2.2.1 and manifested by 5 – 8 Å separation of the formed O-adatoms. These hot adatoms either react with neighboring CO (=αCO_2) or are accommodated before they react from their thermalized ground state with higher activation energy (=βCO_2). This concept is further supported by the observations that the relative proportions of α- and β-CO_2 may be controlled by the O_2 and CO coverages.

5.2.2.8 Particles coming off the surface

The energy and momentum content of particles coming off the surface reflect the exchange of energy between the different degrees of freedom during interaction with the surface and thus the deviations from transition state theory. Particles with full thermal accommodation would exhibit populations of their translational, rotational and vibrational degrees of freedom given by Boltzmann distributions with the surface temperature T_S and a cosine angular distribution. Since the sticking coefficient usually deviates from unity, the principle of microscopic reversibility then requires that this condition is also not fulfilled. State-resolved molecular beam experiments together with classical trajectory calculations shed much light on these processes of energy exchange [68].

As an example for these kinds of investigation, Fig. 12a shows time-of-flight (TOF) distributions from NO molecules in various rotational states (J") coming off an oxidized Ge surface after scattering of a rotationally cold molecular beam with a narrow translational energy distribution centered at 730 meV [61]. The TOF data (lower panel of *a*) exhibit two maxima with short and long mean flight times (i.e. high and low mean kinetic energies) arising from molecules which underwent either direct inelastic scattering or were intermediately adsorbed and then desorbed again, respectively. The latter possess a mean translational energy of 45 meV, independent of their rotational state (curve (b) in Fig. 12b), equal to 2 kT_S. The population of the rotational levels of this part follows a Boltzmann distribution with T_{rot} = 190 K which is again identical to the surface temperature T_S. This is obviously the fraction of molecules undergoing adsorption/desorption. The fast molecules, on the other hand, do not exhibit a Boltzmann distribution of their rotational population, but exhibit a 'rotational rainbow' with overpopulation of the higher J". Their kinetic energy decreases linearly with rotational energy (curve (a)), but to a lesser extent than if the rotational energy would only originate from the primary translational energy (this would give rise to curve (c)). An adequate theoretical description was presented by Mulhausen et al. [70].

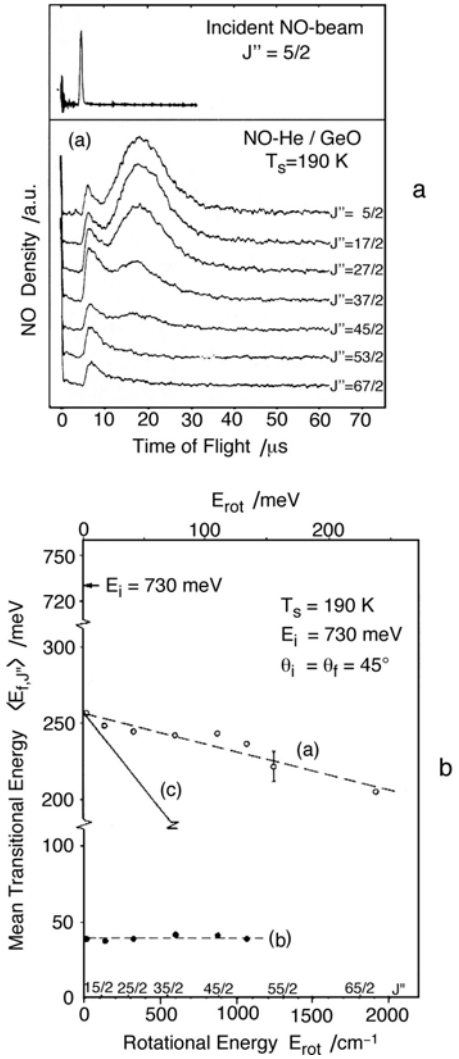

Fig. 12: Scattering of NO molecular beams from an oxidized Ge surface [69].
a: Time-of-flight (TOF) distributions of the incident and scattered molecules in various rotational states J"
b: Correlation between mean translational energy and rotational energy for the part of molecules undergoing direct-inelastic scattering (a) and for those from trapping/desorption (b).

Apart from the reductions of the populations of the various degrees of freedom from thermal equilibrium with the surface of particles coming off the surface as already discussed in sect. 5.2.2.3 ('cooling in desorption'), reaction products resulting from exothermic surface processes may, on the other hand, also carry off excess energy.

If, for example, NO_2 decomposes at a Ge surface, the rotational distribution of the NO molecules formed is non-Boltzmann and independent of surface temperature. This is a clear indication that NO is released directly into the gas phase without intermediate thermal equilibrium with the surface, which effect is attributed to the large exothermicity of the reaction $NO_{2,g} \rightarrow O_{ad} + NO_g$ [71].

More direct evidence for formation of hyperthermal product molecules is obtained by recording their angular (and velocity) distributions as summarized recently by Matsushima et al. [72]. The schematic (one-dimensional) potential diagram for CO oxidation on Pt(111) (proceeding in the thermal ground state through the Langmuir-Hinshelwood mechanism) is depicted in Fig. 13 [73]. The product molecule CO_2 is only very weakly bound to the surface and hence experiences a repulsive potential after passing the transition state and is presumably not fully accommodated before released into the gas phase. As a result the angular distribution follows a $\cos^9\Theta$ relation, rather than $\cos\Theta$ for thermal equilibrium, and the mean translational energy can increase to 330 meV, about tenfold the thermal value [74]. It is suggested that the transition state is bent while the final molecule is linear, and hence also noticeable excitation of internal degrees of freedom is to be expected, and this has indeed been observed by infrared chemiluminescence [75-80]. As an example, Fig. 14 shows the average vibrational temperature and rotational temperature (a), as well as of the antisymmetric stretch vibrational and bending vibrational temperature (b) for CO_2 formed on a Pd(110) surface at a surface temperature T_S = 600 K as a function of the CO/O_2 ratio [80]. These data clearly indicate that the asymmetric stretch vibration is much more highly excited than the other vibrational modes which effect may, in addition, be affected by the composition of the adlayer through interactions between the adsorbed particles [81].

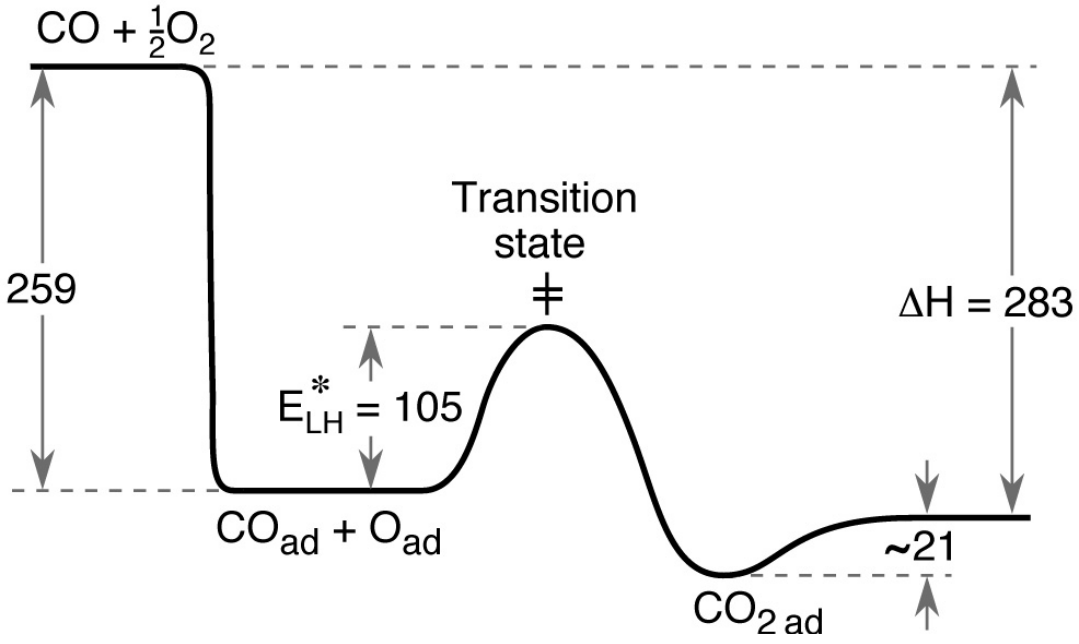

Fig. 13: Schematic potential diagram for CO oxidation on a Pt(111) surface at low coverages [73].

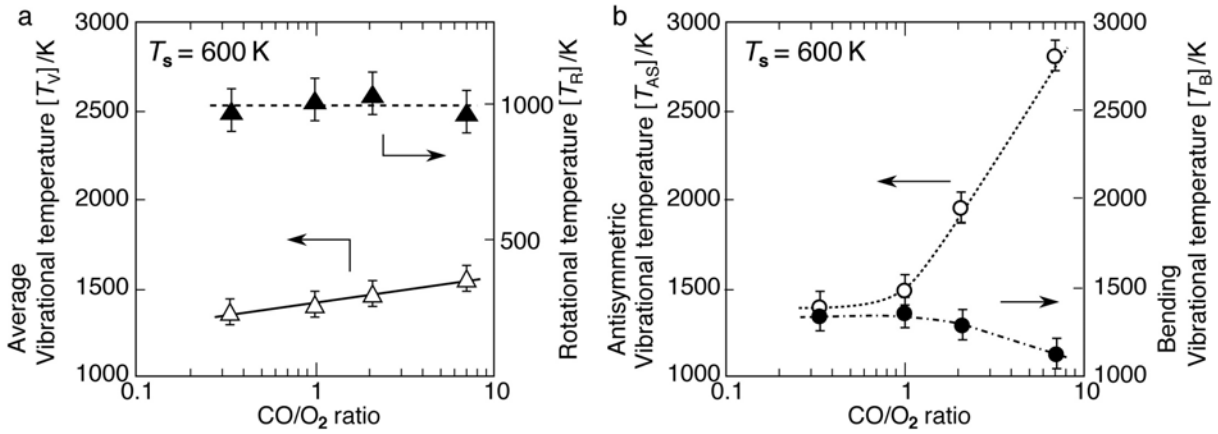

Fig. 14: Chemiluminescence in the CO oxidation on a Pd(110) surface [80].
a: Average vibrational temperature and rotational temperature as a function of the CO/O_2 ratio at Ts = 600 K
b: Temperatures of the antisymmetric and the bending vibrations, respectively, as a function of the CO/O_2 ratio

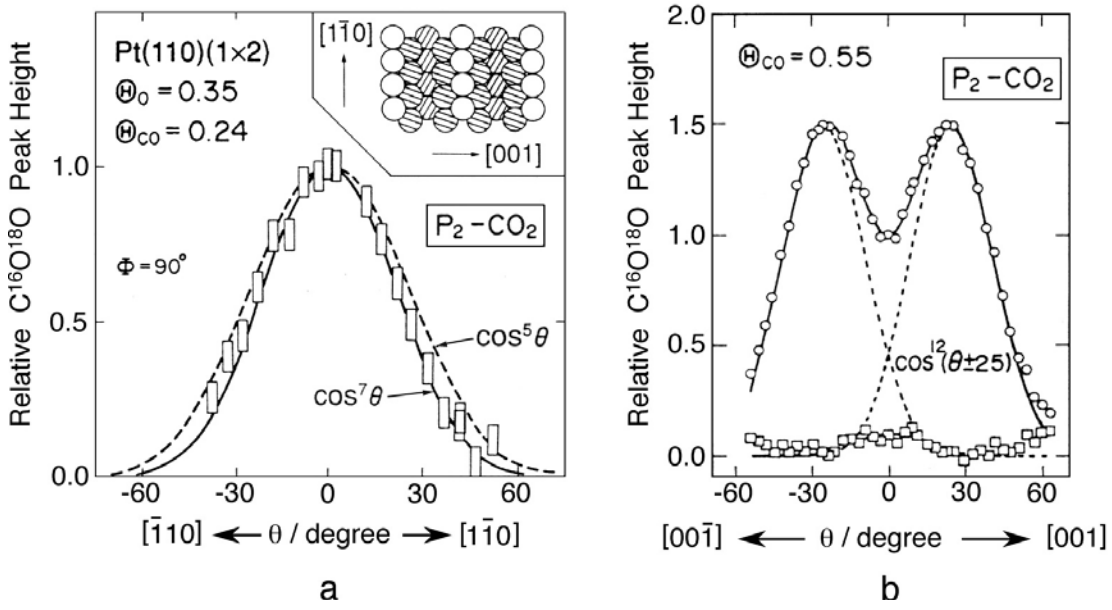

Fig. 15: Polar angle distributions for CO2 formed by CO oxidation on Pt(110) along the [110] and [001] directions, respectively [81].

Fig. 15 shows polar angle distributions of CO_2 formed on Pt(110) along the [110] and [001] directions, respectively [82]. This surface is reconstructed into a 1x2 missing row structure as depicted in the inset of Fig. 15a. The angular distribution along the trough, i.e. the [110]-direction, (Fig. 15a) is peaked along the surface normal, whereas along the [001]-direction (Fig. 15b) it exhibits two maxima at $\pm 35°$. This suggests that CO_2 formation takes place preferentially on the inclined facets of the reconstructed Pt(110) surface, whereby, however, site switching may take place upon variation of the CO coverage [88].

5.2.2.9 Electronic excitations caused by surface reactions

Langmuir and Kingdon [84] observed that heating up a Cs covered W surface causes desorption of Cs^+ ions which effect is easily explained by the fact that it costs less energy to ionize a Cs atom (3.9 eV) than one gains by transferring this electron to the Fermi level of tungsten (~5 eV) . Less obvious, however, is the interpretation of other earlier reports, whereafter interaction of alkali metals with oxygen (and other electronegative species) may cause the emission of electrons [85]. This effect of 'exoelectron' emission has to be attributed to the energy gain associated with the chemical transformation of the surface, and sometimes even the ejection of negative ions is observed [86]. These effects can be rationalized in the framework of a model proposed by Kasemo et al. [87] as illustrated by Fig. 16. The lowest lying empty electronic level (=affinity level) E_A (0.4 eV below the vacuum level E_V for O_2) of a particle is continuously lowered upon approaching the surface. When it crosses the Fermi level E_F, there is a high probability for occupation by an electron tunneling from E_F ('harpooning'), and then the negative ion is further accelerated towards the surface where bond formation takes place. There exists, however, a small probability that the particle will be stopped before it ionizes. The empty level will then be at ε_A which may be occupied by an electron from the metal, and the energy released excites another electron via the Auger effect. Obviously, this exoelectron attains its maximum kinetic energy if both electrons originate from E_F (and $E_{kin,max} = -\varepsilon_A$), and its minimum kinetic energy will be given by the work function, $E_{kin,min} = \phi$. This concept is nicely verified by the experimental data reproduced in Fig. 17: Panel a shows the yield of electrons and panel b the variation of ϕ as a function of O_2 exposure for a Li surface reacting with O_2 [88]. The energy distributions of the emitted electrons at the three stages marked in (b) are plotted in panel c. These data demonstrate that the low-energy cutoff is determined by the work function, while the distributions exhibit a common high-energy leading edge given by ε_A. The yield rises with O_2 exposure due to the continuous decrease of ϕ until a maximum is reached near saturation.

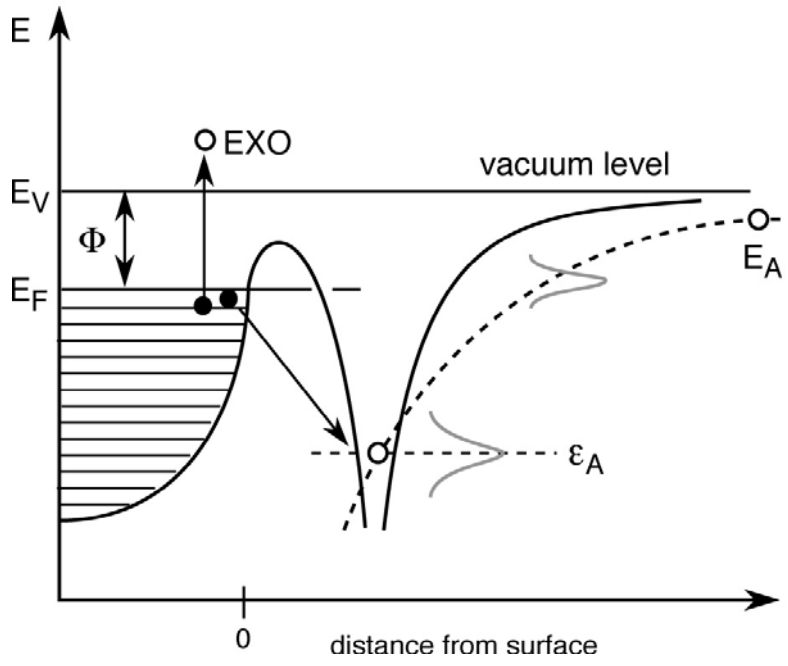

Fig. 16: Electronic energy diagram for an electronegative particle approaching a metal surface giving rise to exoelectron emission [87].

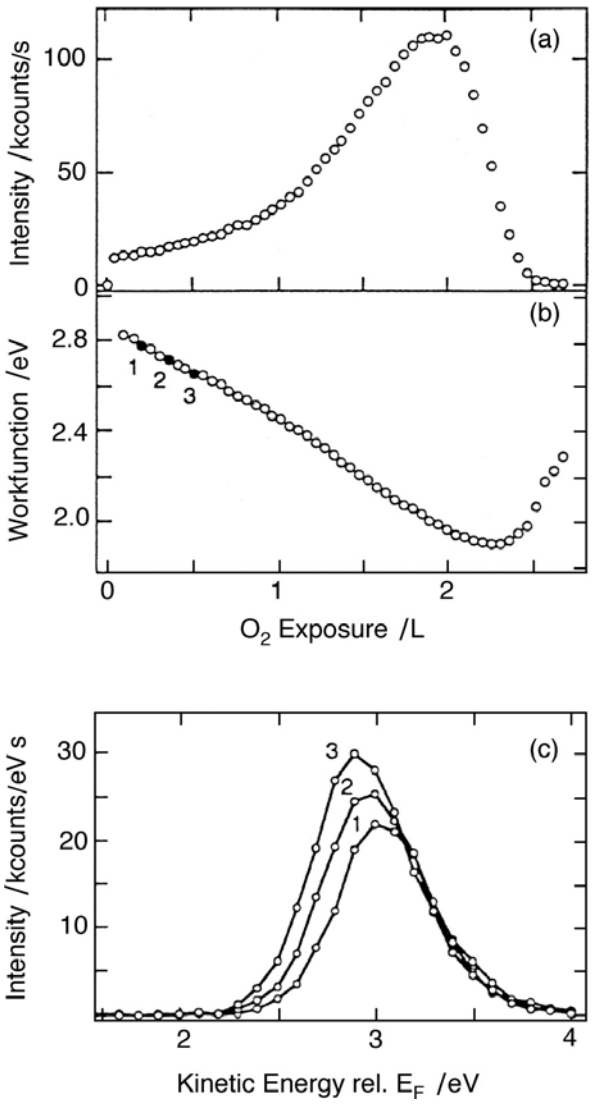

Fig. 17: Exoelectron emission in the reaction of O2 with a Li surface [88].
a: Yield of emitted electrons as a function of O2 exposure
b: Change of the work function as a function of O2 exposure
c: Kinetic energy distributions of the emitted electrons as the 3 stages marked in b.

Such a nonadiabatic pathway will presumably exhibit only a small probability, since the quenching of electronic excitations at metal surfaces occurs much faster than nuclear motion, and with the O_2/Li system the probability for exoelectron emission is only of the order $<10^{-6}$. The competition between nuclear and electronic motion is nicely reflected by the exponential increase of the yield of electron emission with the velocity of the impinging molecules as depicted in Fig. 18 for the system O_2 + Cs [89]. Note that a velocity of $2x10^3$ m/s corresponds to a path of 2 Å within 100 fs, just of the order of the time scale for full relaxation as discussed at the beginning of this chapter

The mechanism illustrated by Fig. 16 suggests that apart from Auger decay deexcitation may also occur via light emission. Fluorescene was indeed observed in the interaction of Cl_2 with K surfaces, but with considerably lower yield than exoelectron emission [90], in agreement with general experience about competition between fluorescence and Auger deexcitation at metal surfaces.

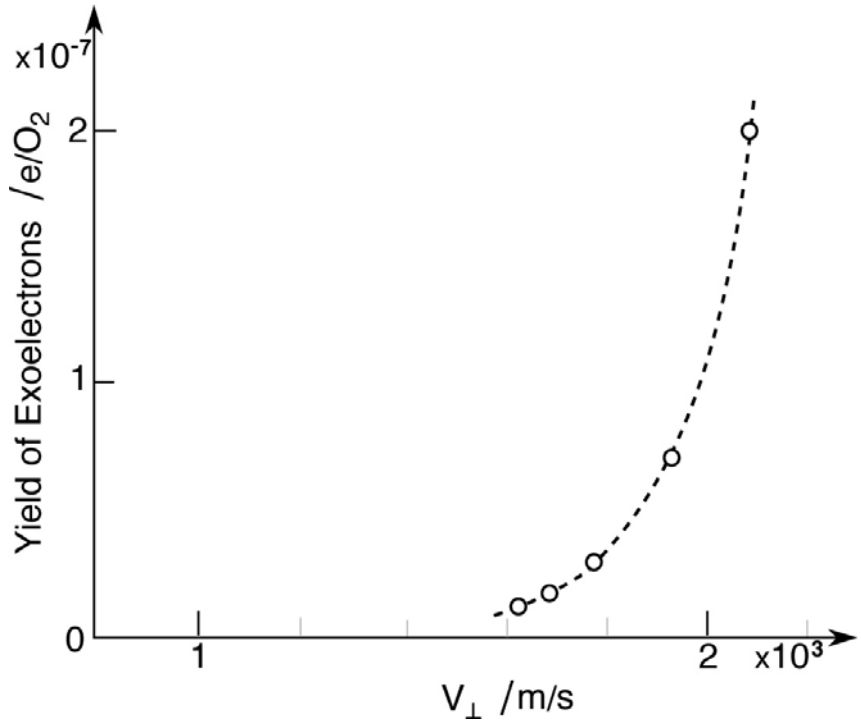

Fig. 18: Variation of the initial intensities of exoelectron emission in the system O_2+Cs with the normal velocity of the impinging O_2 molecules [89].

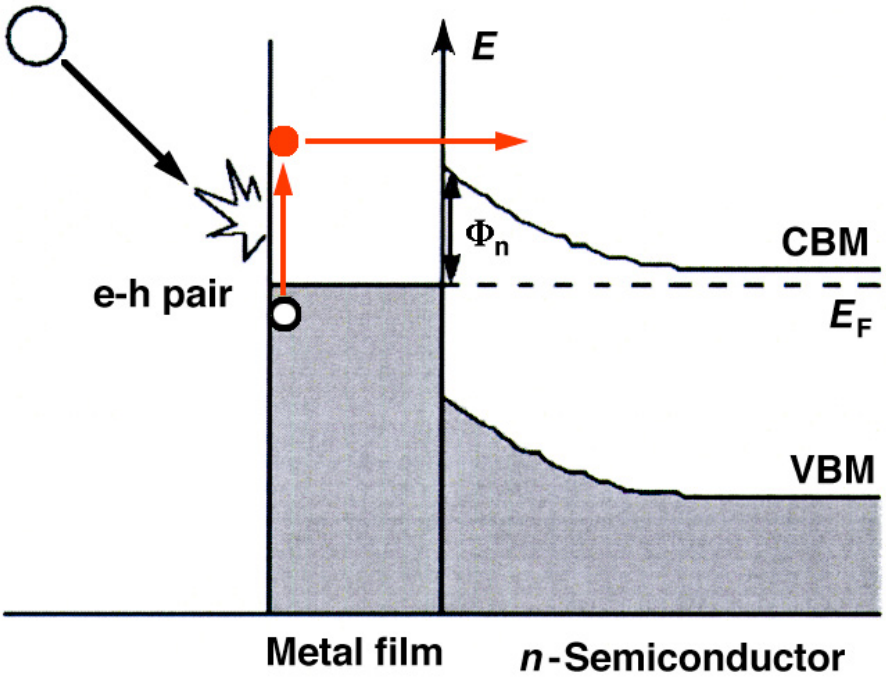

Fig. 19: Mechanism of detecting an electric current as a consequence of electronic excitation by catalytic reaction at the outside of a metal-semiconductor system forming a Schottky barrier [92].

Emission of exoelectrons as a consequence of electronic excitations in the course of a surface reaction will be restricted to the interaction of electronegative molecules with low-work-function metal surfaces, since according to Fig. 16 $\phi < |\varepsilon_A|$ will be a necessary condition. But even then the majority of excitations will arise from combinations of lower-lying electronic states so that the energies of the excited electrons are below the vacuum level and these cannot escape. The creation of such hot electrons could, however, be demonstrated by the use of thin metal films deposited onto a semiconductor surface thus forming a Schottky barrier. This was first shown for Ag and Cu films on a Si(111) substrate forming a Schottky barrier of 0.6 eV height and interacting with H and D atoms [91]. As sketched by Fig. 19, hot electrons formed by reaction at the outer surface can travel through the metal film, cross the Schottky barrier (which replaces the work function in the case of exoelectron emission into vacuum), and can then be recorded as "chemicurrent".

Similar effects have in the meantime been observed with a variety of other systems [92-95]. Recently even continuous electron flow associated with steady-state catalytic oxidation of CO on Pt films forming Schottky diodes on top of TiO_2 [96] and GaN [97] substrates was observed. The reported high current efficiency (3 electrons for production of 4 CO_2 molecules) seems, however, doubtful and requires further confirmation. In general it has, nevertheless, to be concluded that nonadiabatic energy dissipation through transient creation of electron-hole pairs might indeed play a significant role in all surface reactions.

5.2.2.10 Surface reactions initiated by electronic excitations

The example of associative desorption of hydrogen from a Ru(0001) surface initiated by absorption of intense fs-IR laser pulses as discussed in sect. 5.2.2.2 is a clear case for a surface reaction triggered by electronic excitation. Irradiation with higher energy photons (typically with energies up to 6.4 eV) opens up the field of surface photochemistry. The lifetimes of electronic excitations at metal surfaces rapidly decrease with energy above E_F to values of only few fs [98] and are therefore much shorter than the time scales for nuclear motion (~ps). Photochemical reactions seem hence to be rather improbable. This is, however, compensated by the much larger cross section for absorption of the incident light. The latter process occurs predominantly in an about 10 nm thick layer below the surface. The created hot electrons may be transiently attached to an empty adsorbate-derived level and thus cause an electronic excitation of the adsorbate bond eventually leading to chemical transformation. This principle is illustrated by Fig. 20 and underlies the general mechanism of desorption induced by an electronic transition (DIET) [99-101] as described by the so-called MGR model [102,103].

Photodesorption has been studied with a number of systems [99,101,104-106] from which only some results for ammonia desorbing from Cu(111) upon irradiation with 6.4 eV photons will be shortly outlined [107]. Up to a laser fluence of 8 J/cm^2, the desorption yield increases linearly with fluence, indicating that this process is initiated by single photon absorption rather than by heating up the electron gas. Ammonia molecules coming off the surface are strongly peaked along the surface normal and exhibit a mean translational energy of about 0.1 eV which is far in excess of the thermal energy corresponding to the surface temperature of 100 K. A pronounced isotope ef

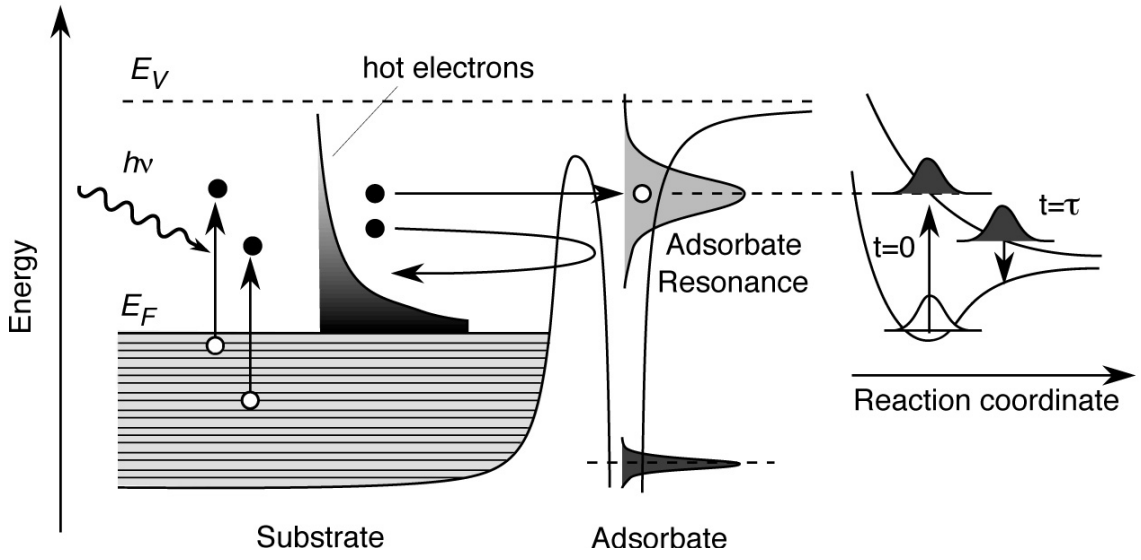

Fig. 20: Energy diagram for an adsorbate-covered metal surface under the influence of light absorption.

fect in the yields of NH_3 vs. ND_3 desorption suggests that the energy required to break the molecule-surface bond is acquired in an intramolecular (i.e. N-H) coordinate during the short-lived electronic excitation, and detailed analysis reveals that this comprises the N-H umbrella mode of vibration [99,105-110].

Instead of being ejected into the gas phase, photogenerated particles may also travel along the surface as 'hot' adparticles, and the formation of CO_2 upon irradiation of a $CO+O_2$ adlayer on Pt(111) provided the first evidence for such a mechanism [111]. More detailed studies with this system [112] revealed that CO_2 formed this way at 25 K substrate temperature exhibited a maximum kinetic energy of 1.35 eV, close to the exit channel's exoergicity (1.45 eV). Photochemical dissociation of adsorbed O_2 is believed to result from transient capture of an excited metal electron into the $3\sigma_u^*$ state, and the transient ion is then attracted to the surface while its bond is elongated [113-115]. For the fastest 'hot' O adatoms a kinetic energy of about 0.7 eV was estimated [116].

The photochemical DIET processes at low light intensities are characterized by a linear relation between yield and laser fluence, indicating a mechanism governed by single-photon excitation: Before the next photogenerated electron arrives, the excited adsorbate complex has already relaxed back into its ground state unless reaction has occurred. With higher light intensities (such as with the fs laser experiments) the adsorbate complex may be excited again before it is quenched [119]. By a sequence of multiple excitation-quenching cycles, the system may climb up the ladder of vibrational levels and eventually undergo desorption, a process first identified with CO/Cu(111) [118] and denoted as 'desorption induced by multiple electronic transitions' (DIMET) [119]. In addition, a conceptually alternative, nonadiabatic mechanism was proposed [120] whereafter the electronic system is coupled to the adsorbate vibrations via electronic friction. Since with high laser fluences the high density of hot electrons equilibrates internally very rapidly (<100 fs), the electron gas can be represented by an electronic temperature T_{el} which differs from the lattice temperature T_{ph} and the adsorbate temperature T_{ad}. This concept was already used in the discussion of sect. 5.2.2.2.

The MGR model underlying the mechanism of DIEF was originally developed for interpreting surface reactions caused by direct impact of low energy electrons (electron stimulated desorption). This effect provides the

most direct evidence for the initiation of chemical transformations at metal surfaces by electronic excitation and has been widely investigated [121].

If instead of an electron gun the tip of a scanning tunneling microscope (STTM) is used as a source for electronic excitations exciting new possibilities arise for probing adsorbate dynamics on atomic scale. After first applications in which atomic motion was manipulated [122-124] also the dynamics of energy exchanges between different degrees of freedom was explored. For the system O_2/Pt(111) tip-induced dissociation [125] as well as rotation [126] was studied. The energy barrier for the latter process was estimated to be about 0.15 eV, while that for dissociation is about 0.4 eV. These results demonstrate the complexity of the overall potential surface and their reaction pathways.

Coupling between different modes was demonstrated with acetylene adsorbed on Cu(100) [127]. Excitation of the C-H stretch mode at 358 meV by tunneling electrons led to a tenfold increase in rotation rate. Detailed analysis revealed, however, that the efficiencies of the process are very low, presumably because of the much more efficient damping of nuclear motions by electronic excitations of the substrate. Similar experiments showing the induction of nuclear motion or dissociation were performed with other weakly held adsorbates at very low temperatures [128,129].

Analogous experiments with more tightly held adsorbates require higher bias voltages and have also been extensively investigated [130-134]. Recently, chlorobenzene adsorbed on a Si(111) surface was in this way subject to selective dissociation of C-Cl bonds, and it was concluded that in this case a two-electron mechanism is operating that couples vibrational excitation and dissociative electron attachment steps [135]. This is demonstrated by Fig. 21, which shows that the yield of desorption increases linearly with the electron current (= single electron process), while a second power relation is found for dissociation.

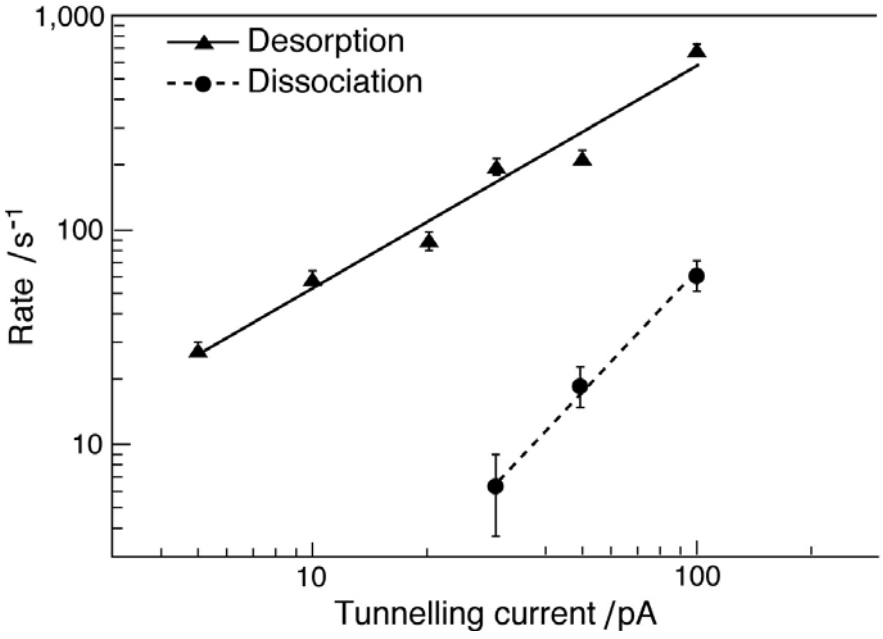

Fig. 21: The rates for desorption and C-Cl bond dissociation, respectively, for chlorobenzene adsorbed on Si(111) as a function of the current between the STM tip and the surface [135].

The reason for the low efficiencies of such processes can be rationalized from the results with the system CO/Cu(111) for which atomic resolution with the STM was combined with the data from ultrafast laser techniques [136]. As sketched by Fig. 22, electrons tunneling from the STM tip to an adsorbed CO molecule can cause their hopping from the surface to the tip if the bias voltage exceeds a threshold value of 2.4 eV. There is again a linear correlation between desorption probability and tunneling current, indicating a single-electron mechanism. Probing the electronic density of states above the Fermi level by two-photon photoelectron spectroscopy revealed that this process involves the transient population of the CO-2π* derived level centered at 3.5 eV above E_F. Thereby transition to a repulsive potential takes place from which desorption according to the DIET mechanism may take place. The desorption probability from this state is extremely small, only about $5x10^{-9}$, suggesting that also its lifetime is very short. Time-resolved two-photon experiments, together with the spectral width of the 2π*-derived level, indicate that this lifetime is indeed less than 5 fs. This result is in accordance with the findings concerning the lifetimes of hot electrons in this energy range in metals [98] and presumably represents the lower bound of the time scale involved in chemical reactions.

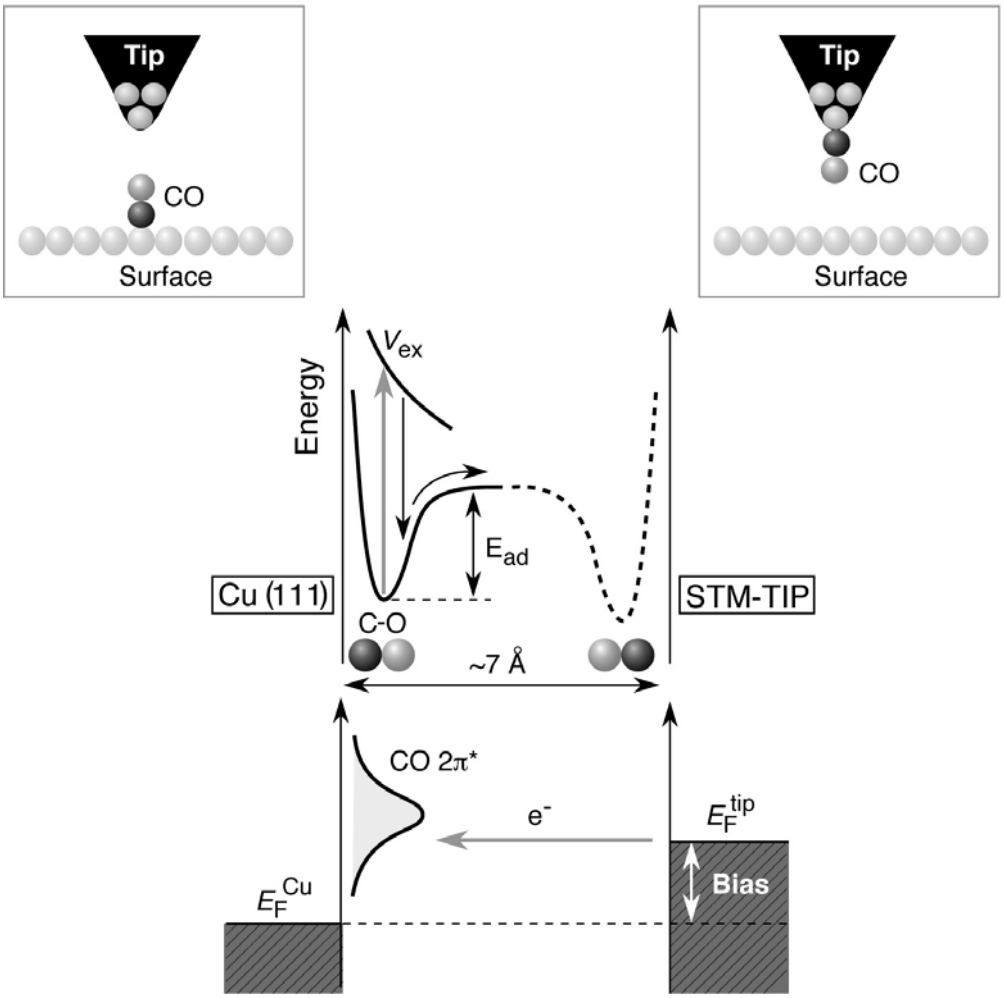

Fig. 22: The mechanism of desorption of a CO molecule adsorbed on Cu(111) by electrons from an opposite STM tip transiently occupying the CO 2π*-derived level [136].

References

1. H. Eyring, M. Polanyi, Z. Phys. Chem.. B **1931**, *12*, 279
2. J. Wintterlin, R. Schuster, G. Ertl, Phys. Rev. Lett. **1996**, *72*, 123
3. B. C. Stipe, M. A. Rezaei, W. Ho, J. Chem. Phys. **1997**, *197*, 6443
4. H. Brune, J. Wintterlin, R. J. Behm, G. Ertl, Phys. Rev. Lett. **1992**, *68*, 624
5. D. N. Denzler, C. Frischkorn, C. Hess, M. Wolf, G. Ertl, Phys. Rev. Lett. **2003**, *91*, 226102
6. D. N. Denzler, C. Frischkorn, M. Wolf, G. Ertl, J. Phys. Chem. B **2004**, *108*, 14503
7. M. Bonn, S. Funk, C. Hess, ,D. Denzler, C. Stampfl, M. Scheffler, M. Wolf, G. Ertl, Science **1999**, *285*, 1042.
8. M. Bonn, C. Hess, S. Funk, J. H. Miners, B. N. J. Persson, M. Wolf, G. Ertl, Phys. Rev. Lett. **2000**, *84*, 4653
9. J. P. R. Symonds, H. Arnolds, D. A. King, J. Phys. Chem. B **2004**, *108*, 14311
10. S. Funk, M. Bonn, D. Denzler, C. Hess, M. Wolf, G. Ertl, J. Chem. Phys. **2000**, *112*, 9888
11. J. C. Tully, Surf. Sci. **1981**, *111*, 461
12. J. Segner, H. Robota, W. Vielhaber, G. Ertl, F. Frenkel, J. Häger, W. Krieger, H. Walther, Surf. Sci. **1983**, *131*, 273
13. H. Robota, W. Vielhaber, M. C. Lin, J. Segner, G. Ertl, Surf. Sci. **1985**, *155*, 101
14. C. T. Rettner, H. A. Michelsen, D. J. Auerbach, J. Chem. Phys. **1995**, *102*, 4625
15. K. D. Rendulic, A. Winkler, Surf. Sci. **1994**, *299/300*, 261.
16. D. Wetzig, M. Rutkowski, R. David, H. Zacharias, Europhys. Lett. **1996**, *36*, 31
17. A. Gross, Surf. Sci. Rep. **1998**, *32*, 291
18. S. T. Ceyer, Ann. Rev. Phys. Chem. **1988**, *39*, 479
19. J. T. Yates, J. J. Zinck, S. Sheard, W. N. Weinberg, J. Chem. Phys. **1979**, *70*, 2266
20. H. Hou, S. J. Gulding, C. T. Rettner, A. M. Wodtke, D. J. Auerbach, Science **1997**, *277*, 80
21. G. Ertl, in Encyclopedia of Catalysis (Ed. I. T. Horvarth), John Wiley **2003**, Vol. 1, 329
22. G. Ertl, S. B. Lee, M. Weiss, Surf. Sci. **1982**, *114*, 515
23. C. T. Rettner, H. Stein, Phys. Rev. Lett. **1987**, *59*, 2768
24. J. J. Mortensen, L. E. Hansen, B. Hammer, J. K. Norskov, J. Catal. **1999**, *182*, 479
25. C. Paglia, A. Nilsson, B. Hernass, O. Karis, P. Bennick, N. Martensson, Surf. Sci. **1995**, *342*, 119
26. P. D. Nolan, B. R. Lutz, P. L. Tanaka, J. E. Davis, C. B. Mullins, Phys. Rev. Lett. **1998**, *81*, 3179
27. J. A. Barker, D. J. Auerbach, Surf. Sci. Rep. **1985**, *4*, 1
28. J. B. Taylor, I. Langmuir, Phys. Rev. **1933**, *44*, 423
29. G. Ehrlich, J. Phys. Chem. **1955**, *59*, 473
30. P. J. Kisliuk, J. Phys. Chem. Solids **1957**, *3*, 95, **1958**, *5*, 78
31. W. H. Weinberg, B. P. Merrill, J. Vac. Sci. Techn. **1972**, *10*, 441
32. J. Harris, B. Kasemo, Surf. Sci. **1981**, *105* L281
33. J V. Barth, T. Zambelli, J. Wintterlin, G. Ertl, Chem. Phys. Lett. **1997**, *270*, 152
34. C. T. Au, H. W. Roberts, Nature **1986**, *319*, 206
35. A. F. Carley, P. R. Davies, M. W. Roberts, Phil. Trans. R. Soc. A **2005**, *363*, 820
36. J. D. Beckerle, Q. Y. Yang, A. D. Johnson, S. T. Ceyer, J. Chem. Phys. **1987**, *86*, 7236
37. J. D. Beckerle, A. D. Johnson, Q. Y. Yang, S. T. Ceyer, J. Chem. Phys. **1989**, *91*, 5756
38. J. Libuda, G. Scoles, J. Chem. Phys. **2000**, *112*, 1522
39. G. Szulczewski, R. J. Lewis, J. Chem. Phys. **1993**, *98*, 5974; **1994**, *101*, 11070
40. C. Akerlund, I. Zoric, B. Kasemo, J. Chem. Phys. **1994**, *104*; 7359; **1998**, *109*, 866
41. C. Akerlund, I. Zoric, B. Kasemo, A. Cupolillo, F. Buatier de Mongeot, M. Rocca, Chem. Phys. Lett. **1997**, *270*, 157
42. T. Engel, G. Ertl, J. Chem. Phys. **1978**, *69*, 1267
43. C. B. Mullins, C. T. Rettner, D. J. Auerbach, J. Chem. Phys. **1991**, *95*, 8649
44. C. Wei, G. L. Haller, J. Chem. Phys. **1996**, *105*, 810
45. M. Kori, B. L. Halpern, Chem. Phys. Lett. **1984**, *110*, 223
46. J. Ree, Y. H. Kim, H. K. Shin, J. Chem. Phys. **1996**, *104*, 742
47. C. T. Rettner, Phys. Rev. Lett. **1992**, *69*, 383
48. C. T. Rettner, D. J. Auerbach, J. Chem. Phys. **1996**, *104*, 2732

49. G. Eilmsteiner, A. Winkler, Surf. Sci. **1996**, *104*, 2732
50. P. Kratzer, J. Chem. Phys. **1997**, *106*, 6752
51. M. Persson, B. Jackson, J. Chem. Phys. 1995, 102, 1078
52. G. Eilmsteiner, W. Walkner, A. Winkler, Surf. Sci., **1996**, *352*, 263
53. Th. Kammler, J. Lee, J. Küppers, J. Chem. Phys. **1997**, *106*, 7362
54. S. Wehner, J. Küppers, J. Chem. Phys. **1998**, *108*, 3353
55. Th. Kammler, S. Wehner, J. Küppers, J. Chem. Phys. **1998**, *109*, 4071
56. Th. Kammler, D. Kolovos-Velliantis, J. Küppers, Surf. Sci. **2000**, *460*, 91
57. T. Zecho, A. Guttler, X. W. Sha, D. Lemoine, B. Jackson, J. Küppers, Chem. Phys. Lett. **2002**, *366*, 188
58. A. Dinger, C. Lutterloh, J. Küppers, J. Chem. Phys. **2001**, *114*, 5338
59. D. Kolovos-Velliantis, J. Küppers, Surf. Sci. **2004**, *548*, 67
60. T. Kammler, J. Küppers, J. Phys. Chem. B **2001**, **105**, 8369
61. D. Kolovos-Velliantis, T. Kammler, J. Küppers, Surf. Sci. **2001**, *482*, 166
62. D. Kolovos-Velliantis, J. Küppers, J. Phys. Chem. B **2003**, *107*, 2564
63. J. Biener, E. Lang, C. Lutterloh, J. Küppers, J. Chem. Phys. **2002**, *116*, 3063
64. D. D. Eley, E. K. Rideal, Nature **1940**, *146*, 401
65. K. H. Allers, H. Pfnür, P. Feulner, D. Menzel, J. Chem. Phys. **1994**, *100*, 3985
66. T. Matsushima, Surf. Sci. **1983**, *127*, 403
67. C. E. Wartnaby, A. Stuck, Y. Y. Yeo, D. A. King, J. Chem. Phys. **1995**, *102*, 1855
68. J. A. Barker, D. J. Auerbach, Surf. Sci. Rep. **1985**, *4*, 1
69. A. Mödl, T. Gritsch, F. Budde, T. J. Chuang, G. Ertl, Phys. Rev. Lett. **1986**, *57*, 384
70. C. W. Muhlhausen, L. R. Williams, J. C. Tully, J. Chem. Phys. **1985**, *83*, 2594
71. A. Mödl, H. Robota, J. Segner, W. Vielhaber, M. C. Lin, G. Ertl, Surf. Sci. **1986**, *169*, L341
72. T. Matsushima, I. Rzeznicka, Y. Ma, Chem. Rec. **2005**, *5*, 81
73. C. T. Campbell, G. Ertl, H. Kuipers, J. Segner, J. Chem. Phys. **1980**, *73*, 5862
74. K. H. Allers, H. Pfnür, P. Feulner, D. Menzel, J. Chem. Phys. **1994**, *100*, 3985
75. D. A. Mantell, S. B. Ryali, B. L. Halpern, G. L. Haller, J. B. Fenn, Chem. Phys. Lett. **1981**, *81*, 185
76. G. W. Coulston, B. L. Haller, J. Chem. Phys. **1991**, *95*, 6932
77. C. Wei, G. L. Haller, J. Chem. Phys. **1996**, *105*, 810
78. K. Kunimori, H. Uetsuka, T. Iwade, T. Watanabe, S. Ito, Surf. Sci. **1993**, *283*, 58
79. H. Uetsuka, K. Watanabe, K. Kunimori, Surf. Sci. **1996**, *363*, 73
80. K. Nabao, S. Ito, K. Tamishige, K. Kunimori, Chem. Phys. Lett. **2005**, *410*, 86
81. V. P. Zhdanov, Surf. Sci. **1986**, *165*, L31
82. T. Matsushima, J. Chem. Phys. **1990**, *93*, 1464
83. S. Han, T. Matsushima, Phys. Chem. Chem. Phys. (PCCP) **2005**, *7*, 651
84. I. Langmuir, K. H. Kingdon, Phys. Rev. **1923**, *21*, 381
85. F. Haber, G. Just, Ann. Phys. **1909**, *30*, 411; **1911**, *36*, 308
86. T. Greber, Surf. Sci. Rep. **1997**, *28*, 1
87. B. Kasemo, E. Törnqvist, J. K. Nørskov, B. Lundqvist, Surf. Sci. **1979**, *89*, 554
88. K. Hermann, K. Freihube, T. Greber, A. Böttcher, R. Grobecker, D. Fick, G. Ertl, Surf. Sci. **1994**, *113*, L806
89. A. Böttcher, A. Morgante, T. Giessel, T. Greber, G. Ertl, Chem. Phys. Lett. **1994**, *231*, 119
90. L. Hellberg, J. Strömqvist, B. Kasemo, B. L. Lundqvist, Phys. Rev. Lett. **1995**, *74*, 4742
91. H. Nienhaus, H. S. Bergh, B. Gergen, A. Majundar, W. H. Weinberg, E. W. McFarland, Phys. Rev. Lett. **1999**, *82*, 446
92. B. Gergen, H. Nienhaus, W. H. Weinberg, E. W. McFarland, Science **2001**, *294*, 2521
93. H. Nienhaus, B. Gergen, W. H. Weinberg, E. W. McFarland, Surf. Sci. **2002**, *514*, 172
94. B. R. Cuyene, H. Nienhaus, E. W. McFarland, Phys. Rev. B **2004**, *70*, 115322
95. S. Glass, H. Nienhaus, Phys. Rev. Lett. **2004**, *93*, 168302
96. X. Ji, A. Zuppero, J. M. Gidwani, G. A. Somorjai, Nano Lett. **2005**, *5*, 753
97. X. Ji, A. Zuppero, J. M. Gidwani, G. A. Somorjai, J. Am. Chem. Soc. **2005**,, *5*, 753
98. E. Knoesel, A. Hotzel, T. Hertel, M. Wolf, G. Ertl, Surf. Sci. **1996**, *368*, 76
99. F. M. Zimmermann, W. Ho, Surf. Sci. Rep. **1995**, *22*, 127
100. J. W. Gadzuk, in „Femtochemistry“ (J. Manz and L. Wöste, eds.) Verlag Chemie, Weinheim **1994**
101. S. M. Harris, S. Holloway, C. R. Darling, J. Chem. Phys. **1995**, *102*, 8235

102. D. Menzel, R. Gomer, J. Chem. Phys. **1964**, *41*, 3311
103. P. R. Redhead, Can. J. Phys. **64**, *42*, 886
104. X. L. Zhou, X. Y. Zhu, J. M. White, Surf. Sci. Rep. **1991**, *13*, 73
105. H. L. Dai, Witto (eds) „Laser specroscopy and photochemistry at metal surfaces“, World Scientific, Singapore, **1995**
106. H. Petek, S. Ogawa, Progr. Surf. Sci. **1998**, *56*, 239
107. T. Hertel, M. Wolf, G. Ertl, J. Chem. Phys. **1995**, *102*, 3414
108. E. Hasselbrink, M. Wolf, S. Holloway, P. Saalfrank, Surf. Sci. **1996**, *263*, 179
109. H. Guo, T. Seideman, J. Chem. Phys. **1995**, *103*, 9062
110. K. H. Bornscheuer, W. Nessler, M. Binetti, E. Hasselbrink, P. Saalfrank, Phys. Rev. Lett. **1997**, *78*, 1174
111. W. D. Mieher, W. Ho, J. Chem. Phys. **1989**, *91*, 4755
112. V. A. Ukraintsev, I. Harrison, J. Chem. Phys. **1992**, *96*, 6307
113. X. Y. Zhu, S. R. Harch, A. Campion, J. M. White, J. Chem. Phys. **1989**, *91*, 5011
114. F. Weik, A. de Meijere, E. Hasselbrink, J. Chem. Phys. **1993**, *99*, 682
115. I. Harrison, Acc. Chem. Res. **1998**, *31*, 631
116. A. N. Artsyukhovich, I. Harrison, Surf. Sci. **1996**, *350*, L199
117. R. E. Walkup, D. M. Newns, Ph. Avouris, Phys. Rev. B **1993**, *48*, 1858
118. J. A. Prybyla, A. W. K. Tom, G. D. Aumiller, Phys. Rev. Lett. **1992**, *68*, 503
119. J. A. Misewich, S. Nakabayashi, P. Weigund, M. Wolf, T. F. Heinz, Surf. Sci. **1996**, *363*, 204
120. M. Brandbyge, P. Hedegard, T. F. Heinz, J. A. Misewich, D. M. Newns, Phys. Rev. B **1995**, *52*, 6042
121. N. H. Tolk, M. M. Traum, J. C. Tully, T. E. Madey (eds.), „DIET I“, Springer, Berlin **1983**, and subsequent volumes of this series
122. J. A. Stroscio, D. Eigler, Science **1991**, *254*, 1319
123. Ph. Avouris, Acc. Chem. Res. **1995**, *28*, 95
124. L. Bartels, G. Meyer, K. H. Rieder, Phys. Rev. Lett. **1997**, *79*, 697
125. B. C. Stipe, M.A. Rezaei, W. Ho, S. Gao, M. Persson, B. I. Lundqvist, Phys. Rev. Lett. **1997**, *78*, 4410
126. B. C. Stipe, M. A. Rezaei, W. Ho, Science, **1998**, *27*, 1907
127. B. C. Stipe, M. A. Rezaei, W. Ho, Phys. Rev. Lett. **1998**, *81*, 1263
128. T. Komeda, Y. Kim, M. Kawai, B. N. J. Persson, H. Ueba, Science **2002**, *195*, 2055
129. J. I. Pascual, N. Lorentz, Z. Song, H. Conrad, H. P. Rust, Nature **2003**, *423*, 525
130. F. W. Fishlock, A. Oral, R. G. Egdelt, J. B. Pethica, Nature **2000**, *404*, 743
131. L. J. Lauhon, W. Ho, Phys. Rev. Lett. **2000**, *84*, 1527
132. S. W. Hla, L. Bartels, G. Meyer, K. H. Rieder, Phys. Rev. Lett. **2000**, *85*, 2797
133. P. H. Lu, J. C. Polanyi, D. Rogers, J. Chem. Phys. **1999**, *111*, 9905
134. L. Soukiassan, A. J. Mayne, M. Carbone, G. Dujardin, Phys. Rev. B **2003**, *68*, 035303
135. P. A. Sloan, R. E. Palmer, Nature **2005**, *434*, 367
136. L. Bartels, G. Meyer, K. H. Rieder, D. Velic, E. Knoesel, A. Hotzel, M. Wolf, G. Ertl, Phys. Rev. Lett. **1998**, *80*, 2004